

https://dspace.org/

Seismic imaging of the complex geological structures in the southwestern edge of the Western limb Bushveld Complex through focusing prestack depth migration of the legacy 2D seismic data

Mpofana Sihoyiya; F Hloušek; Musa Manzi; Moyagabo Rapetsoa; S Buske ...

WILEY-BLACKWELL
https://hdl.handle.net/10539/43079
WOS

Downloaded from a DSpace repository. https://dspace.org/

Check for updates

Received: 9 June 2023 | Accepted: 14 June 2024

DOI: 10.1111/1365-2478.13569

Geophysical Prospecting | EAGE EUROPEAN ASSOCIATION OF GEOSCIENTISTS & ENGINEERS

ORIGINAL ARTICLE

Seismic imaging of the complex geological structures in the southwestern edge of the Western limb, Bushveld Complex through focusing pre-stack depth migration of legacy 2D seismic data

Mpofana Sihoyiya[1] | **Felix Hloušek**[2] | **Musa S. D. Manzi**[1] | **Moyagabo K. Rapetsoa**[1] | **Stefan Buske**[2] | **David Khoza**[3]

[1]School of Geosciences, University of the Witwatersrand, Johannesburg, South Africa

[2]Institute of Geophysics and Geoinformatics, TU Bergakademie Freiberg, Freiberg, Germany

[3]Council for Geoscience, Pretoria, South Africa

Correspondence
Musa S. D. Manzi, University of the Witwatersrand, Johannesburg, South Africa.
Email: musa.manzi@wits.ac.za

Abstract

We reprocessed a 50-km long legacy 2D reflection seismic profile acquired in 1986, under a project funded by the National Geophysics Program to improve the delineation of complex geological structures that host the platinum-bearing horizons (known as the UG2 reef; a chromitite horizon) on the south-eastern edge of the Western limb of the Bushveld Complex and to investigate the continuity of the reef below the thick cover. The pre-stack seismic data quality was improved through conventional processing steps. We applied standard Kirchhoff pre-stack depth migration as well as advanced coherency migration techniques. Both imaging techniques yielded good structural images of the platinum deposits, their hanging wall and footwall rocks. In particular, the coherency migration technique has provided significantly better images in complex faulted regions, yielding a better understanding of the interrelationship between fault activity and platinum deposit distribution, and the relative chronology of tectonic events. Moreover, the regional geological structures (Crocodile River fault and Chaneng structure) that crosscut the profile are clearly defined.

KEYWORDS
data processing, imaging, seismics, tomography, velocity analysis

INTRODUCTION

The Paleoproterozoic age (2.06 Ga) Bushveld Complex (Figure 1a) is the world's largest igneous intrusion (~64,000 km^2), which is associated with the platinum-group element (PGE) deposits of South Africa (Manzi, Cooper et al., 2019). The Bushveld Complex PGEs occur within the mafic stratiform horizons locally known as reefs (Basson, 2019; Sehoole et al., 2020). These deposits are mined from the outcrop on the complex margin to depths as great as 2.3 km concealed beneath cover rocks. Between the 1970s and 1980s, traditional greenfield approaches of mineral exploration (mainly geological mapping, exploration drilling and potential field methods) were successfully employed to map the extent of the Bushveld Complex. To date, mature brownfield mineral exploration requires innovative and novel geological and geophysical techniques to improve the delineation of deeply buried platinum-bearing horizons (Donoso

This is an open access article under the terms of the Creative Commons Attribution-NonCommercial License, which permits use, distribution and reproduction in any medium, provided the original work is properly cited and is not used for commercial purposes.
© 2024 The Author(s). *Geophysical Prospecting* published by John Wiley & Sons Ltd on behalf of European Association of Geoscientists & Engineers.

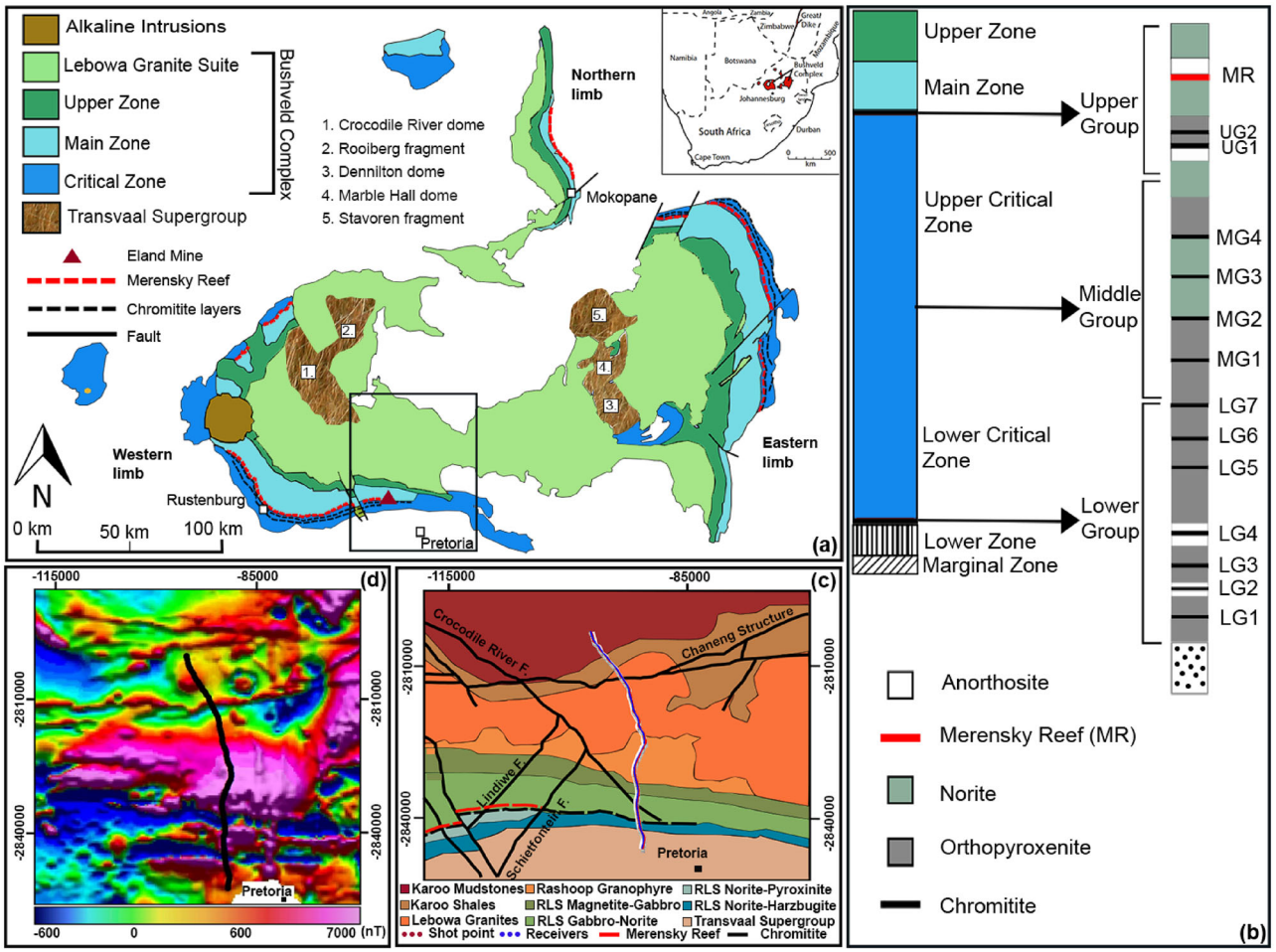


FIGURE 1 (a) Simplified geological map of the Bushveld Complex showing the study area, (b) simplified stratigraphy of the Bushveld Complex, (c) geological map covered by the seismic line and (d) aeromagnetic map covered by the line.

et al., 2020; Manzi, Cooper et al., 2019). However, these methods are not widely used because they are deemed to be expensive and cost beyond the exploration budget of some mining companies. Consequently, companies that revise and improve their existing data stand to benefit (Malehmir et al., 2019; Manzi, Malehmir et al., 2019).

Revision and re-processing of legacy reflection seismic data have been utilized successfully by several authors (e.g., Donoso et al., 2020; Malehmir & Bellefleur, 2010; Manzi, Cooper et al., 2019; Manzi, Malehmir et al., 2019; Sihoyiya et al., 2022; Westgate et al., 2020, and references therein) for hard rock mineral exploration. Challenges presented by these data sets are related to bad storage and documentation, such as outdated tapes and hard copies, respectively. Several pre-processing steps are needed to correct inaccurate coordinates and set up new geometry. Despite these challenges, these data are still valuable, cost-effective and have the potential to be revised and reworked (Malehmir et al., 2019), particularly in the Bushveld Complex where the PGE mineralization was first recognized in 1924 with the discovery of the first economically viable PGE deposit (Cawthorn, 1999; Manzi, Cooper et al., 2019). In the 1980s, the 3D reflection seismic method was introduced in the Bushveld Complex, and since then a seismic database with tens of 2D and 3D seismic surveys has been acquired across the Complex to delineate the platinum-bearing horizons and geological structures under thick cover rocks (Manzi, Malehmir et al., 2019; Pretorius et al., 2000, 2003).

In this study, we reprocessed a 50-km long, 16 s two-way traveltime (TWT) legacy 2D reflection seismic profile acquired on the southeastern edge of the Western limb of the Bushveld Complex. The complex is subdivided into four different limbs, namely the Northern, Eastern, Southern, and Western limbs. Most PGE deposits in the Western limb are associated with the Critical Zone (Figure 1a,b) of the Rustenburg Layered Suite. The Critical Zone diminishes in thickness from west to east (Rustenburg to Pretoria), and this diminution has resulted in a lack of interest in mineral exploration in the southeastern edge of the Western limb, near Pretoria (Cawthorn & Webb, 2001; Scheiber-Enslin & Manzi, 2018; Sehoole et al., 2020). The main aim of the study is to improve the delineation of the ore-bearing horizons and

13652478, 2024, 7, Downloaded from https://onlinelibrary.wiley.com/doi/10.1111/1365-2478.13569 by South African Medical Research, Wiley Online Library on [30/11/2024]. See the Terms and Conditions (https://onlinelibrary.wiley.com/terms-and-conditions) on Wiley Online Library for rules of use; OA articles are governed by the applicable Creative Commons License

the complex geological structures of the Bushveld Complex. This is accomplished by applying careful reprocessing workflows (mainly pre-stack depth-imaging) on the 1986 legacy seismic profile to produce improved seismic images for a better understanding of the continuity of the platinum-bearing horizons on the southeastern edge of the Western limb, as well as the tectonic evolution of the geological structures in general. The legacy seismic line was collected from south to north (Figure 1c), traversing towards the centre of the complex. Improved imaging of the centre of the complex could provide insight regarding the connectivity between the Western and Eastern limbs of the Bushveld Complex (Cawthorn & Webb, 2001; Shithigona et al., 2018).

In addition to the reprocessing of the 2D legacy seismic profile, we integrate the aeromagnetic data to gain an understanding of the geological structures and their relationship with the platinum-bearing horizon. The regional high-resolution aeromagnetic data (Figure 1d) are used to provide constraints on the geometry of the faults and magnetic dykes that crosscut the legacy seismic line (Scheiber-Enslin & Manzi, 2018). Herein, we demonstrate a suitable depth imaging workflow through reprocessing of the 1986 data with a special attention on pre-stack depth migration (PSDM). We compare the results from two PSDM methods: conventional Kirchhoff pre-stack depth migration and a focusing PSDM technique, namely coherency migration (CM). This is to demonstrate the effectiveness of the focusing migration technique in the hardrock environment.

The ray-based focusing PSDM techniques have a common objective of restricting the Kirchhoff migration operator to the physically pertinent region in the subsurface. They mainly differ in the implementation of the restriction and velocity model consideration (Buske et al., 2009). Some techniques are loosely defined by tapering the migration operator using a definite cosine taper (Tillmanns & Gebrande, 1999). Others make a full use of the physical concepts of Gaussian beams, Fresnel zones, anisotropy or analogous wavefield approaches (Bleistein, 1984; Hua & McMechan, 2009; Lüth et al., 2005; Sun & Schuster, 2003; Tabti et al., 2004; Takahashi, 1995). In this study, we applied CM, which reconstructs for each imaging point of the specular diffraction surface in the recorded wavefield and estimates the coherency at neighbouring traces (Neidell & Taner, 1971), and uses these values for weighting (Hloušek et al., 2015b).

ELAND MINE AND WESTERN LIMB OF THE BUSHVELD COMPLEX

Background information

The Eland mine (triangle in Figure 1a) is a relatively new platinum mine on the southeastern edge of the Western limb of the Bushveld Complex. The mine started with opencast mining operations in 2007, and underground production commenced in 2010 until placed under care and maintenance approximately 5 years later. Potgieter and Malan (2010) detailed the mining method at the Eland platinum mine, and one of the complicating factors is the dip of the ore body at ∼18° to the North. In 2019, Eland mine assessed the feasibility of extending the infrastructure to access reserves down dip and along the strike of the platinum-bearing horizons, with a hybrid mining method (a semi-mechanized development as well as traditional stopping). Eland mine is currently mining the Merensky reef (MR) and the UG2, and the Merensky is not well developed on the eastern edge of the mining rights area. The underdevelopment of the MR is due to the thinning of the Critical Zone from west to east in the Western limb. Consequently, on the eastern edge, Eland mine conducted a feasibility study to employ an open-pit mining operation. Therefore, we envision that the results from this legacy seismic profile could provide insight into understanding the thinning of the Critical Zone further east (∼10 km east of the Eland mine).

Geological background

The Western limb of the Bushveld Complex has been studied by several authors, including Cawthorn and Webb (2001), Manzi, Malehmir et al. (2019) and Sehoole et al. (2020), Scheiber-Enslin and Manzi (2018). However, the southeastern edge of the Western limb has not been studied in detail due to thinning of the mineralized Critical Zone (Cawthorn & Webb, 2001). Figure 1b shows a simplified stratigraphic column of the Western limb of the Bushveld Complex. Summarily, the mafic cumulate rocks of the Bushveld Complex are called the Rustenburg Layered Suite (RLS) and are divided into five zones, namely the Marginal, Lower, Critical, Main, and Upper. The RLS overlies the Transvaal Supergroup sediments and is in turn overlain by the felsic cumulate rocks of the Bushveld Complex called the Rashoop Granophyre Suite and Lebowa Granite Suite (Scheiber-Enslin & Manzi, 2018). The Critical Zone of the RLS, reaching a maximum thickness of ∼1.5 km, is divided into Lower and Upper Critical Zones according to the plagioclase crystal's appearance (Sehoole et al., 2020). The two economically viable platinum-group element deposits in the study area, MR and UG2, occur near the top of the Upper Critical Zone. MR is hosted within the Merensky pyroxenite between 15 and 400 m above the UG2 chromitite and has a thickness range of 0.5–2 m (Manzi, Malehmir et al., 2019; Rapetsoa et al., 2022).

Structurally, the southeastern edge of the Western limb is characterized by a major right-lateral Crocodile River fault trending NNW. This fault is accompanied by NNE trending mafic dykes with low magnetic signature and minor NE

13652478, 2024, 7, Downloaded from https://onlinelibrary.wiley.com/doi/10.1111/1365-2478.13569 by South African Medical Research, Wiley Online Library on [30/11/2024]. See the Terms and Conditions (https://onlinelibrary.wiley.com/terms-and-conditions) on Wiley Online Library for rules of use; OA articles are governed by the applicable Creative Commons License

trending left-lateral scissor faults such as Lindiwe and Schietfontein faults (Figure 1c) (Bosson, 2019). Basson (2019) interpreted these fault structures to postdate the Bushveld Complex mineralized mafic units, as well as being hinged by the Crocodile River fault on the northeastern edge and exhibit maximum displacement of approximately 150 m on the southwestern edge. The Crocodile River fault is particularly interesting since it crosscuts the 1986 legacy seismic profile in the south (Figure 1c). Another large-scale EW trending geological lineament of interest is the strongly magnetized Chaneng structure (Figure 1c,d) that crosscuts the legacy profile in the north. The Chaneng structure is a normal fault with a magnetic signature that is associated with a dyke (Basson, 2019; Scheiber-Enslin & Manzi, 2018). The imaging of these structures through reprocessing of the legacy seismic data is significant for future mine planning and characterization of their geometry in the region.

Transvaal Supergroup inliers

The Bushveld Complex mafic and granitic rocks intruded the Transvaal Supergroup, and several inliers of highly deformed Transvaal rocks occur in the Bushveld Complex (Figure 1a). The Crocodile River dome and the Rooiberg fragment in the Western limb and Dennilton-Marble Hall dome, and Stavoren fragment in the Eastern limb are the most prominent Transvaal Supergroup inliers (Hartzer, 1995). Understanding the geology and tectonic evolution of these inliers provides insight into the distribution and geometry of the target mineralized RLS and regional tectonics of the Bushveld Complex. The Crocodile River dome lithostratigraphy and tectonic relationship with the Bushveld Complex is of interest in this study because it forms the northern half of the reprocessed legacy profile. Several authors (e.g. Hartzer, 1989, 1995; Humphrey, 1906, 1909, and references therein) provide a detailed geological description of the dome, which is over 1560-m thick (Hartzer, 1995).

LEGACY 2D SEISMIC DATA

Seismic data acquisition

We received the 50-km long 2D legacy reflection seismic profile as raw shot gathers and a cropped post-stack migrated image with acquisition information in hardcopy observer's reports. The raw shot gathers were in SEG-Y format without geometry information in the header files, which required manual digitizing from the observer's reports. The profile was collected on the southeastern edge of the Western limb of the Bushveld Complex, approximately 10 km east of the Eland mine. Table 1 outlines the summary of the acquisition parameters of the profile. The 2D legacy reflection seismic profile was acquired in 1986 as part of the National Geophysics Programme (Durrheim, 2015) using three Vibroseis trucks as energy source. We recovered a total of 998 correlated shot records with 96 active channels per shot, 50 m shot spacing and 25 m receiver spacing. The survey was designed with a 16-s sweep length, 20–90 Hz linear sweep frequency band and a sampling interval of 2 ms. The profile was acquired with a split spread geometry with a near offset of 112.5 m, a far offset of 1287.5 m and 24-fold coverage. The geophones used were Sercel SM4U single component with dominant frequency of 10 Hz.

TABLE 1 Legacy profile acquisition parameters.

Survey parameters	
Survey type	2D crooked line
Year	1986
Length	50 km
Direction	S–N
Spread	Split spread: 1287.5–112.5 m × 112.5–1287.5 m. 96 active channels
Nominal fold	24
Recording system	
Recording device	MDS-10, 96 channel
Sample rate	2 ms
Recording length	21 s
Sweep length	16 s
Sweep frequency range	20–90 Hz
Source information	
Source device	3 Vibroseis
Vibrator controller	P II
Source spacing	50 m
Receiver information	
Receiver spacing	25 m
Geophone type	10 Hz (SM4U)

Seismic data reprocessing

The seismic profile was initially processed through a conventional post-stack time migration workflow (Odgers et al., 1993). In this study, we applied a pre-stack depth imaging workflow (Figure 2). Moreover, the key element of the workflow is the application of an advanced focusing pre-stack depth-migration approach (coherency migration [CM]) as well as the usage of a reliable migration velocity model in depth. The velocity analysis is carried out conventionally by picking semblance peaks from a velocity spectrum

13652478, 2024, 7, Downloaded from https://onlinelibrary.wiley.com/doi/10.1111/1365-2478.13569 by South African Medical Research, Wiley Online Library on [30/11/2024]. See the Terms and Conditions (https://onlinelibrary.wiley.com/terms-and-conditions) on Wiley Online Library for rules of use; OA articles are governed by the applicable Creative Commons License

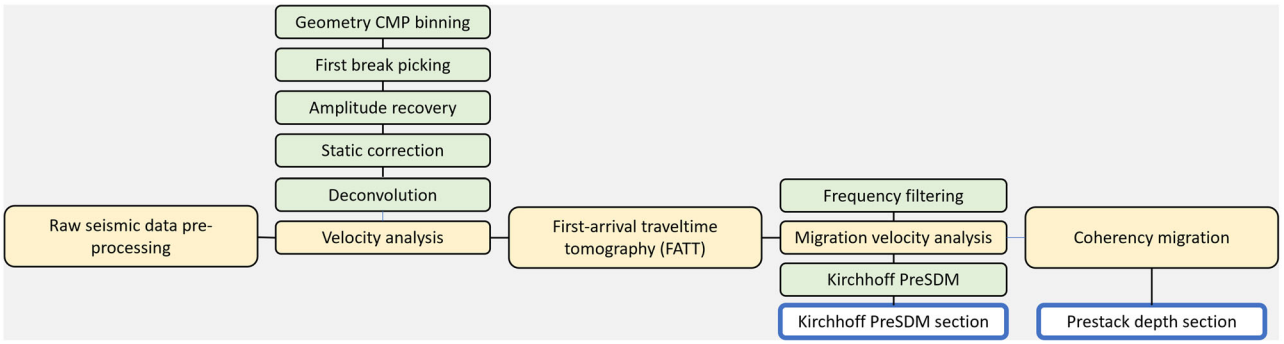


FIGURE 2 Summary of the depth imaging workflow.

to determine the moveout velocity assuming a horizontally layered medium. However, semblance velocity analysis cannot be easily adapted to hardrock environments that have strong lateral velocity variations and steeply dipping reflectors. The results from using the wrong velocity model for the normal moveout correction strongly affect the quality of the stacked section. In this study, the velocity model used for prestack depth migration (PSDM) is a smoothed interval velocity model derived from constant velocity stacks spanning every hundredth common midpoint (CMP).

A summary of the processing workflow applied to the data set is shown in Figure 2. The legacy data were recovered and resorted through various pre-processing steps to enhance it to contemporary standards compatible with modern seismic processing software. The header information was digitized from handwritten observer's reports to set up a new geometry with traces stored in CMP bins spaced 12.5-m apart using a spline curve. A 50-Hz notch filter was applied to the data during acquisition to remove the spiking noise resulting from the AC power lines in the study area.

Figure 3 shows an example of raw and reprocessed shot gathers. The data generally have good quality with most shot gathers showing clear first breaks (indicated by the FB arrow in Figure 3a). Following the geometry setup of the data, a total of 89,882 first arrivals were manually picked for the application of appropriate statics. The floating datum was calculated using a maximum elevation of 1368 m as a fixed datum with a replacement velocity of 6000 m/s. The statics were calculated with the RMS error of less than 7 ms using the least-squares inversion method (Woodward, 1991). The attenuated amplitudes were amplified using an automatic gain control with a window length of 1000 ms.

Additionally, we applied f–k filtering, spiking deconvolution and frequency filtering. The direct surface wave arrivals have an average velocity of 3200 m/s; therefore, an f–k filter was applied to mute surface waves and any linear signal velocity less than 3300 m/s. We broadened the spectrum using predictive deconvolution with a 4-ms gap length and 180 ms filter length to simulate spiking deconvolution. A frequency bandpass filter was applied to remove frequencies outside the frequency band [5–20–100–110 Hz]. Finally, a refraction top mute was applied to the data. As indicated by reflections A, D and E in Figure 3b, reflection continuity and resolution of the processed shot gathers have improved.

Analysis and comparison between the raw and reprocessed 1986 2D seismic profile sample shot gathers is shown in Figure 3. The strong reflections observed on the exemplary reprocessed shot gather are the main lithological contacts with significant acoustic impedance contrast between the overlying and underlying rocks (Figure 3b): Rashoop Granophyre-Upper Zone ferrogabbros (A), Transvaal Supergroup-Rustenburg Layered Suite norites (D) and an intrusive Diabase sill (E).

Refraction tomography velocity model

Interactive interval velocity analysis was performed for the construction of a migration velocity model in the depth domain. The migration velocity model needs to incorporate realistic information about the near surface as well as deep-seated geology. The near-surface velocity information used in this study is derived directly from refraction tomographic velocity analysis. A conventional velocity analysis was conducted for depths without ray coverage with constant velocities constrained by the previous studies conducted in the Bushveld Complex (Odgers et al., 1993; Rapetsoa et al., 2022).

After manually picking a total of 89,882 P-wave first breaks, a three-layered initial model was defined by fitting the gradients in the first break picks for the first arrival traveltime inversion. Using the geometry of the data, the synthetic traveltimes were calculated for the initial model using the ray tracing method. The tomographic approach that was applied to the data set to calculate synthetic traveltimes is a nonlinear refraction traveltime tomography method developed by Zhang and Toksöz (1998).

A first break traveltime tomography to a depth of 600 m, which accounted for elevation variation to a datum of 1398 m, was computed across the profile with a maximum shot gather

13652478, 2024, 7, Downloaded from https://onlinelibrary.wiley.com/doi/10.1111/1365-2478.13569 by South African Medical Research, Wiley Online Library on [30/11/2024]. See the Terms and Conditions (https://onlinelibrary.wiley.com/terms-and-conditions) on Wiley Online Library for rules of use; OA articles are governed by the applicable Creative Commons License

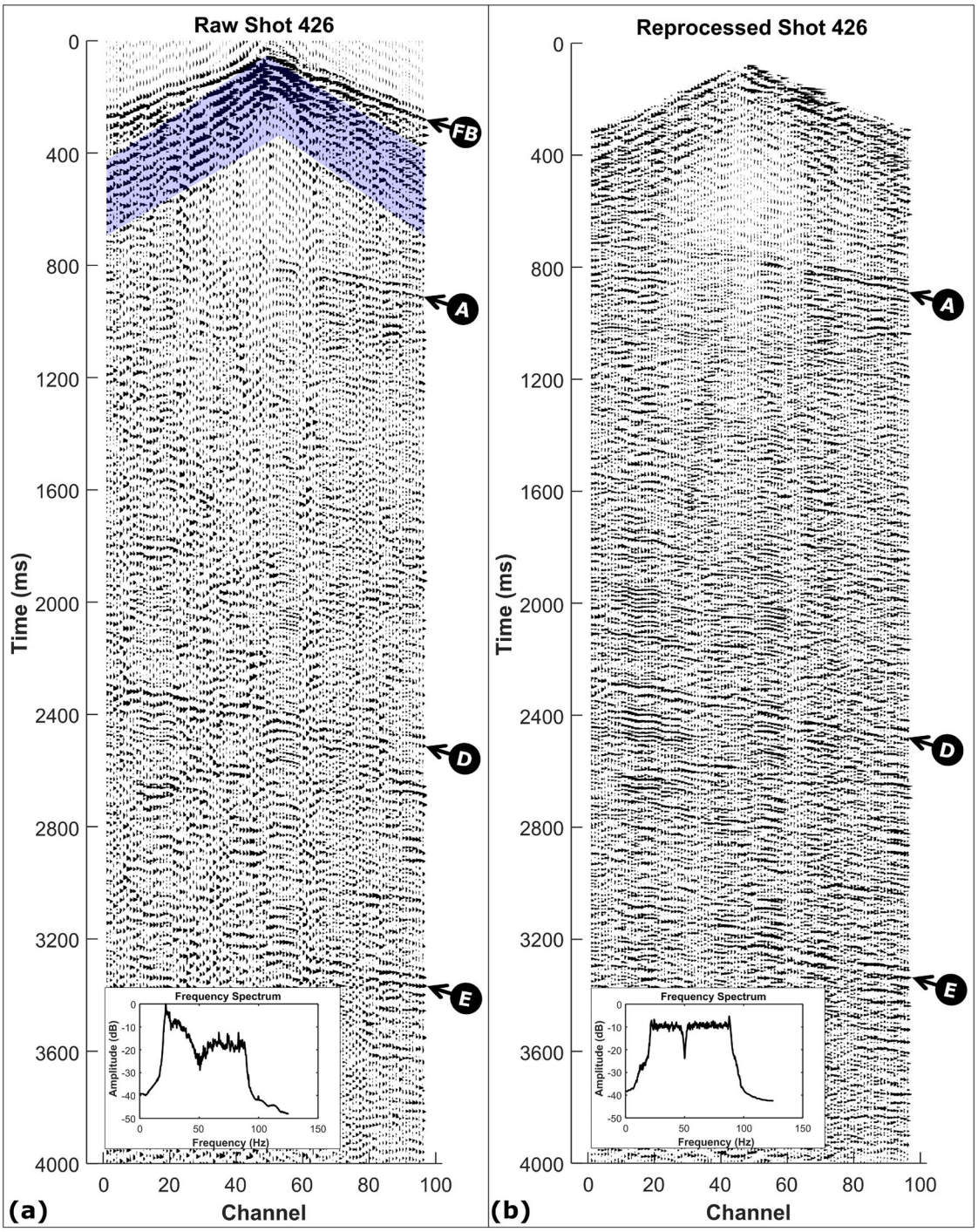


FIGURE 3 Raw (a) versus reprocessed (b) sample shot gathers of the seismic legacy profile, with the raw data shot gather showing clear first breaks (FB). The reprocessed shot gather shows continuous and preserved reflection contacts: Rashoop Granophyre-Upper Zone ferrogabbros (A), Transvaal Supergroup-Rustenburg Layered Suite norites (D) and a Diabase sill (E), as well as attenuated surface waves, shaded blue on the raw shot gather.

offset of ~1200 m and a padding airwave velocity of 340 m/s. The ray paths and velocity model are displayed in Figure 4a,b, respectively, with vertical exaggeration. The velocity model shows low-resolution velocity boundaries between strata with velocities ranging between 2000 and 6800 m/s. The uppermost low-velocity layer of the initial model is relatively thin, only occurring on the southern and northern edges of the profile and possibly represents Karoo cover sediments with velocities ranging from 2500 to 3500 m/s. The second layer has a strong velocity gradient from 3500 to 5500 m/s. The observed strong velocity gradient in the second layer is possibly the weathered layer. The host rocks have an average

13652478, 2024, 7, Downloaded from https://onlinelibrary.wiley.com/doi/10.1111/1365-2478.13569 by South African Medical Research, Wiley Online Library on [30/11/2024]. See the Terms and Conditions (https://onlinelibrary.wiley.com/terms-and-conditions) on Wiley Online Library for rules of use; OA articles are governed by the applicable Creative Commons License

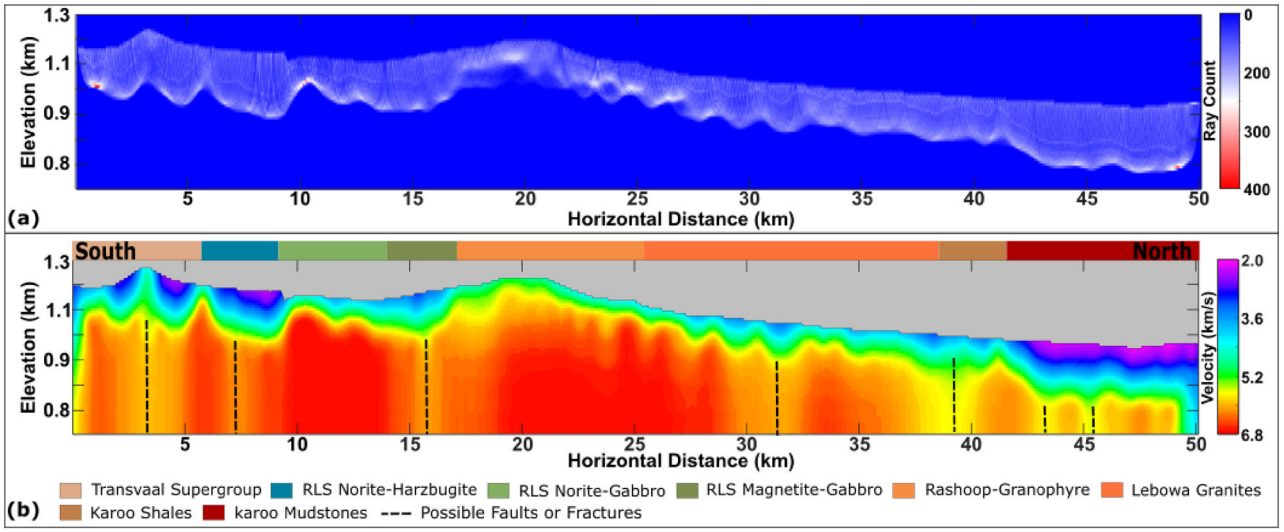


FIGURE 4 Refraction ray path (a), velocity model (b) of the profile, and the surface geological map along the profile.

velocity of 6500 m/s with low-resolution lateral velocity variation characteristic of weak zones, which are interpreted as possible faults or fractures (Figure 4b).

The mapped geological structures are possible extensions of the deeper seated faults mapped on the reflection section, with no direct correlation because of the depth limitation of refraction tomography model. Furthermore, the data were collected using a reflection seismic acquisition technique rather than the conventional seismic refraction tomography acquisition technique, which leads to low resolution at depth (Akingboye & Ogunyele, 2019).

Depth imaging

Seismic imaging in hardrock environments is often more challenging in comparison with softrock settings because of the complex geology, disrupted reflectors and scattered seismic energy. Pre-stack depth migration, especially in a Kirchhoff type implementation, has been successfully applied in such complex crystalline hardrock environments since for at least two decades (Buske, 1999). Further developments towards incorporating a focusing migration operator resulted in advanced pre-stack depth migration techniques, for example Fresnel Volume Migration (Buske et al., 2009; Lüth et al., 2005), CM and coherency-based Fresnel Volume Migration (Hloušek et al., 2015a). Successful applications of these focusing PSDM methods range from imaging crustal fault systems (Hloušek and Buske, 2016), over the characterization of geothermal reservoirs (Hloušek et al., 2015b; Jusri et al., 2018; Riedel et al., 2015; Schreiter et al., 2015), to the high-resolution imaging of mineral deposits (Bräunig et al., 2019; Cheraghi et al., 2022; Heinonen et al., 2019; Hloušek et al., 2022; Singh et al., 2019).

Here, we demonstrate again the effectiveness of these approaches by applying the CM technique to the 2D legacy seismic profile from the Bushveld Complex known for its hardrock platinum-group element exploration.

CM is one of the possible implementations of focusing pre-stack depth migration approaches. It is based on Kirchhoff pre-stack depth migration, which is an integral solution for the wave equation in the form of diffraction integral (Schneider, 1978), written as

$$V(m) = \frac{-1}{2\pi} \int \int_{A} w(m,r) \times \dot{u}\left(r, t_s + t_R\right) \mathrm{d}r. \qquad (1)$$

Therefore, the resultant image value V for a random point $m = m(x, y, z)$ in the subsurface is described by the weighted summation over the corresponding diffraction surface $(t_s + t_R)$ for the given point. Here, t_s and t_R are the traveltimes from source S and receiver R to the image point m, respectively; $\dot{u}$ is the time derivative of the wavefield and r is the distance from image point m to the receiver R. The weighting function $w(m, r)$ along the diffraction curve accounts for the directivity-based energy losses and spherical divergence. The image for a single surface shot wavefield, which is scattered by a single diffraction point in a homogeneous medium and recorded by a single receiver on surface, is constructed by smearing the amplitudes along their corresponding two-way traveltime (TWT) isochrones. This concept can be extended for multiple shots and receivers on surface by treating every single point along the reflector as a point diffractor and a migrated image of the reflector can be constructed by constructive interference of all TWT isochrones along the reflector.

Focusing migration approaches limit the migration operator to the physically relevant part along the TWT isochrone.

13652478, 2024, 7, Downloaded from https://onlinelibrary.wiley.com/doi/10.1111/1365-2478.13569 by South African Medical Research, Wiley Online Library on [30/11/2024]. See the Terms and Conditions (https://onlinelibrary.wiley.com/terms-and-conditions) on Wiley Online Library for rules of use; OA articles are governed by the applicable Creative Commons License

This is achieved by adding an additional weighting factor $f(m,r)$ to the Kirchhoff integral solution (Equation 1) dependent on the image point, which ensures that the amplitudes are smeared in the physically pertinent region along the traveltime isochrone, as follows:

$$V(m) = \frac{-1}{2\pi} \int \int_A f(m,r) \times w(m,r) \times \dot{u}(r, t_s + t_R) \mathrm{d}r. \quad (2)$$

CM uses a weighting factor $f(m,r) = C_c$ obtained directly from the input data (Hloušek et al., 2015b). This weighting factor is computed by evaluating the semblance coefficients of the recorded wavefield along the theoretical diffraction curves, defined by the individual TWT for the same image point at different neighbouring receivers. Neidell and Taner (1971) defined the semblance coefficient to be the normalized input/output energy ratio, where the sum of input traces is the output trace. Mathematically, the ratio of coherent energy and total energy within a time window over a certain number of neighbouring receivers is given by the following equation:

$$f = C_c^p(m,r) = \left(\frac{\int_{-\frac{T}{2}}^{\frac{T}{2}} \left| \sum_{j=0}^{N-1} u_j \left(t_s + t_{R_j} + t \right) \right|^2 \mathrm{d}t}{N \int_{-\frac{T}{2}}^{\frac{T}{2}} \sum_{j=0}^{N-1} \left| u_j \left(t_s + t_{R_j} + t \right) \right|^2 \mathrm{d}t} \right)^p. \quad (3)$$

where p is an exponent factor used to enhance coherent signal, and very high values of p can lead to enhanced migration artefacts; therefore, a careful consideration of values of p is needed. T is the window length which ranges from one to three times the time span of the reflected signal, and N is the number of traces used for comparison. The resultant semblance coefficient can be utilized without modification on the migration integral as it is normalized (i.e. ranging from 0 to 1).

The most critical step in CM is choosing comparison traces because the results are not only dependent on the number of traces (N), but they also depend on the aperture spanned by these traces. Consequently, the boundary condition for the number of traces is set using the maximum offset from the actual trace location. Additionally, the source, image point and receiver geometries are taken into consideration using the projected Fresnel zone as follows:

$$r_{F_{pro}} = \sqrt{\mathrm{d}x^2 + \mathrm{d}y^2 + \mathrm{d}z^2} \sqrt{2 \frac{t_{dom}}{t_0}} \sqrt{\frac{\mathrm{d}x^2 + \mathrm{d}y^2}{\mathrm{d}z^2} + 1}. \quad (4)$$

where the first term is the image point to receiver distance, and the combination of the first and the second term approximates the first Fresnel zone radius on a constant velocity subsurface. t_{dom} represents the dominant period of the source signal, and $t_0 = 2t_R$, where t_R is the traveltime between the image point and receiver. The last term represents the paraxial Fresnel zone projected to the surface at the receiver location. Therefore, Equation (4) provides an additional boundary condition for the comparison traces (N) used in computing the semblance coefficient. The minimum value for the third term is 1, where the image point lies at the receiver location since $\mathrm{d}x^2 + \mathrm{d}y^2 = 0$. Therefore, the approximation is equivalent to the projected Fresnel zone and $r_{F_{pro}}$ is small for an image point that is located near the receiver and increases with increased lateral distance between the receiver and image point (Hloušek et al., 2015b).

RESULTS AND INTERPRETATION

According to the surface geological map (Figure 1c) the 1986 2D seismic profile was collected over an outcrop of the Transvaal Supergroup in the southern portion, Bushveld Complex in the middle portion, and Karoo Sequence in the north portion. The strata are documented to be dipping to the north in the southern section at approximately 20°. This is supported by the presence of Karoo sediments on the northern edge of the data and the outcrop of the Transvaal and Bushveld strata on the southern edge (Odgers et al., 1993). The results of the coherency migration (CM) technique are presented as absolute values of migrated wavefield amplitudes in order to produce robust images that are less affected by erroneous velocities (Tillmanns et al., 1996).

Comparison between legacy data and reprocessed data

The new imaging results (Figures 5b and 6) of the southern section of the legacy profile are in general analogous to the results presented by Du Plessis and Levitt (1987) of an unmigrated stacked section of the profile. Odgers et al. (1993), aiming to collapse diffractions, migrate dipping reflections to their true subsurface position and suppress multiple reverberations, reprocessed the profile and presented a detailed interpretation of the post-stack time migrated section (Figure 5a). The results correspond to the interpretation of the southern section of the CM result (Figure 5b). The high amplitude reflections marked D, E, F and G (Figure 5a,b) correspond to the Transvaal Supergroup reflectors, with reflection D marking the contact between the Transvaal sequence and the overlying Rustenburg Layered Suite (RLS) norites. Reflection E is the 85 m thick Diabase sill, with its continuity clearly mapped by the CM at depth. Reflections F and G mark the base of Timeball Hill Formation and Chuniespoort Group or Black reef, respectively, and their continuity is better imaged by the CM. The contact between the low amplitude reflections of high frequency from the RLS norites and the overlying low amplitude reflections of low

13652478, 2024, 7, Downloaded from https://onlinelibrary.wiley.com/doi/10.1111/1365-2478.13569 by South African Medical Research, Wiley Online Library on [30/11/2024]. See the Terms and Conditions (https://onlinelibrary.wiley.com/terms-and-conditions) on Wiley Online Library for rules of use; OA articles are governed by the applicable Creative Commons License

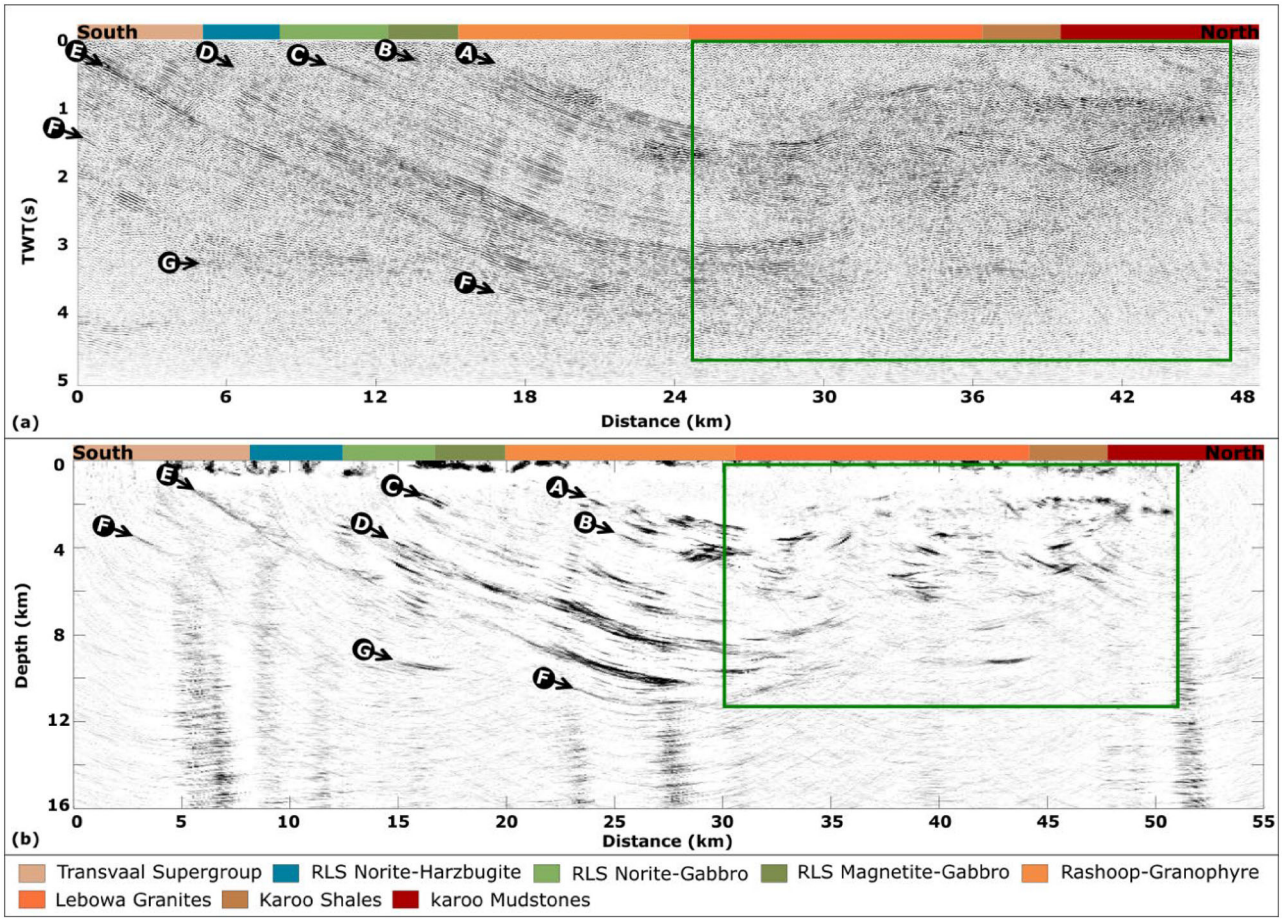


FIGURE 5 Comparison of the post-stack time migrated section (a) (Odgers et al., 1993) and reprocessed coherency migration (CM) depth section (b). The region of notable improvement in the data is outlined by rectangles (see Figure 7 for closeup). The main lithological contacts: Rashoop Granophyre-Rustenburg Layered Suite (RLS) ferrogabbros (A), RLS ferrogabbros-RLS gabbros (B), RLS gabbros-RLS norites (C), Transvaal Supergroup-RLS norites (D), a Diabase sill (E), base of Timeball Hill Formation (F), base of Chuniespoort group (G) as well as the geological outcrop along the profile are shown.

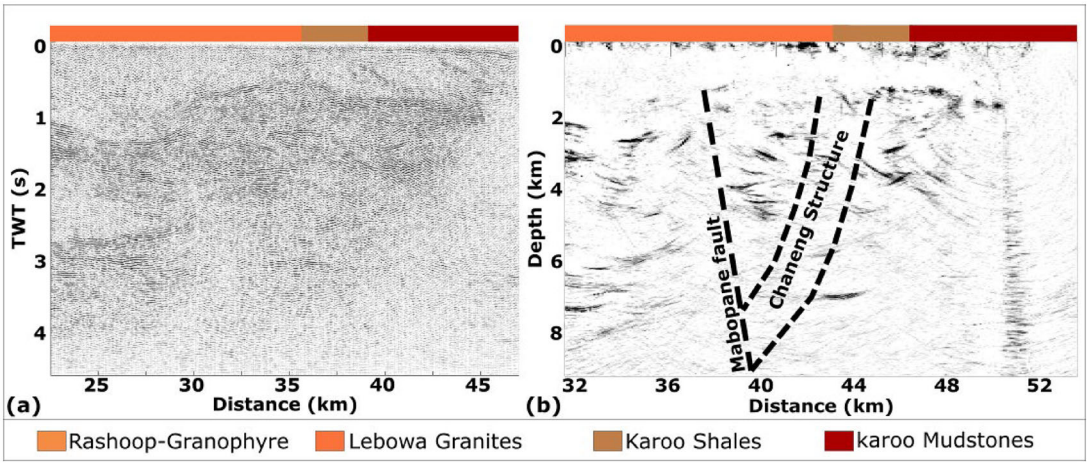


FIGURE 6 Zoomed region of the legacy stack (a) and reprocessed stack (b) as indicated by green rectangles in Figure 5.

13652478, 2024, 7, Downloaded from https://onlinelibrary.wiley.com/doi/10.1111/1365-2478.13569 by South African Medical Research, Wiley Online Library on [30/11/2024]. See the Terms and Conditions (https://onlinelibrary.wiley.com/terms-and-conditions) on Wiley Online Library for rules of use; OA articles are governed by the applicable Creative Commons License

frequency from the RLS gabbros is marked C in Figure 5a,b. Symbols A and B represent the RLS gabbros-RLS ferrogabbros contact and the RLS ferrogabbros-Rashoop Granophyre Suite contact, respectively (Odgers et al., 1993).

The northern section of the profile (Figure 6, highlighted by rectangles in Figure 5) was interpreted with contrasting results by Du Plessis and Levitt (1987) and Odgers et al. (1993). Du Plessis and Levitt (1987) concluded that the RLS rocks terminate against a major fault called Mabopane fault and the geology is analogous to the neighbouring Crocodile River dome. Odgers et al. (1993) interpreted the low signal-to-noise ratio (SNR) character of the northern section of the legacy time migrated profile to be due to out-of-plane reflection energy, poor source-to-ground coupling or energy scattering and interference. Therefore, concluding that the RLS rocks occur as a highly faulted anticlinal structure, which formed during the intrusion of the Bushveld Complex rocks (Odgers et al., 1993). The CM result (Figure 6b) resolved the anticlinal structure better than the legacy post-stack time migrated section (Figure 6a). This region exhibits high amplitude discontinuous reflections overlain by low amplitude discontinuous reflections. The distinction between these reflections is not clear in the legacy stack, whereas the CM image allows for the delineation of major geological structures like the Chaneng structure and the Mabopane fault (Figure 6b). The high amplitude reflections are interpreted to correspond to highly faulted Transvaal Supergroup rocks, and the overlying low amplitude reflections correspond to the RLS norite-gabbros.

Figure 7a,b shows the comparison between the conventional Kirchhoff pre-stack depth migration (KPreSDM) section and the CM section down to a depth of 16 km, with the outcrop data along the profile overlain. The A, B, C, D, E, F and G reflections are clearly defined in the CM section (Figure 7b) compared to the KPreSDM section (Figure 7a).

Aeromagnetic data

The regional aeromagnetic data acquired at a terrain clearance of 100–150 m with flight lines spaced at 1 km imaged the Upper Zone sequence outcrop mapped in the four limbs, due to the strong positive magnetic signature of the ferrogabbro and magnetite horizons as shown in Figure 1d (Campbell, 2011). Figure 8a shows the magnetic profile along the seismic section in Figure 8b, with the geological structures mapped by magnetic data overlain on the seismic section. These data adequately map the regional faults and dykes that crosscut the seismic profile (e.g. the Chaneng structure and the Crocodile River fault). The low magnetic signature observed in the northern section of the profile is interpreted to result from the absence of the positively magnetized rocks of the Upper Zone (RLS Magnetic-Gabbro).

Out-of-plane reflectivity

A 2D reflection seismic line collected with high-fold crooked line geometry is a limited swath 3D survey of the subsurface reflectivity near the line (Nedimovic & West, 2003). Therefore, reflection energy from out-of-plane structures can migrate to the profile imaging plane at later, equal or earlier two-way traveltime compared to energy reflected within plane, depending on their geometry. The reflections from out-of-plane energy can interfere (constructively or destructively) with reflections within plane leading to distorted amplitudes and low SNR. Here, 2D seismic data are pseudo-3D migrated producing a 3D volume (Figure 9) to access cross-profile information about the subsurface reflectivity. The green arrows show constructive interference out-of-plane with ambiguous possible sources of reflectivity. The reflectivity could be from anywhere in the cylindrical curve around the surface. However, this shows that there is a presence of out-of-plane reflectivity in the northern half of the profile contributing to the low SNR.

Figure 9 is a 3D view of the crooked line CM section with the surface geological map (Figure 1c) overlain, and the regional geological structures (e.g. Crocodile River fault and Chaneng structure marked) together with the target platinum-group element reefs (Merensky reef [MR] and UG2). The migration velocity model (Figure 10a) and the final interpreted section of the 2D legacy reflection seismic profile (Figure 10b) are shown in Figure 10. A seismic velocity of 6500 m/s was assigned to the Transvaal Supergroup rocks, and 5700 m/s assigned to the RLS norites from previous studies (Rapetsoa et al., 2022; Scheiber-Enslin & Manzi, 2018). The proposed tectonic evolution along the profile is outlined in Figure 11.

DISCUSSION

The previous interpretation of the profile carried out by Du Plessis and Levitt (1987) and Odgers et al. (1993) was focused primarily on reflection contacts associated with the geological sequences on the post-stack time migrated section correlated to the mapped surface geological outcrop. The dominant reflections, Marked A, B, C, D, E, F and G outlined on the reprocessed data, correspond with the results from the previous interpretation. The geological models were supported by regional gravity data along the profile (Odgers et al., 1993). However, the previous interpretation did not outline detailed tectonic information along the profile and recommended the application of pre-stack depth imaging techniques (Odgers et al., 1993).

The Rustenburg Layered Suite (RLS) sequence of the Bushveld Complex is of particular interest in this study as

13652478, 2024, 7, Downloaded from https://onlinelibrary.wiley.com/doi/10.1111/1365-2478.13569 by South African Medical Research, Wiley Online Library on [30/11/2024]. See the Terms and Conditions (https://onlinelibrary.wiley.com/terms-and-conditions) on Wiley Online Library for rules of use; OA articles are governed by the applicable Creative Commons License

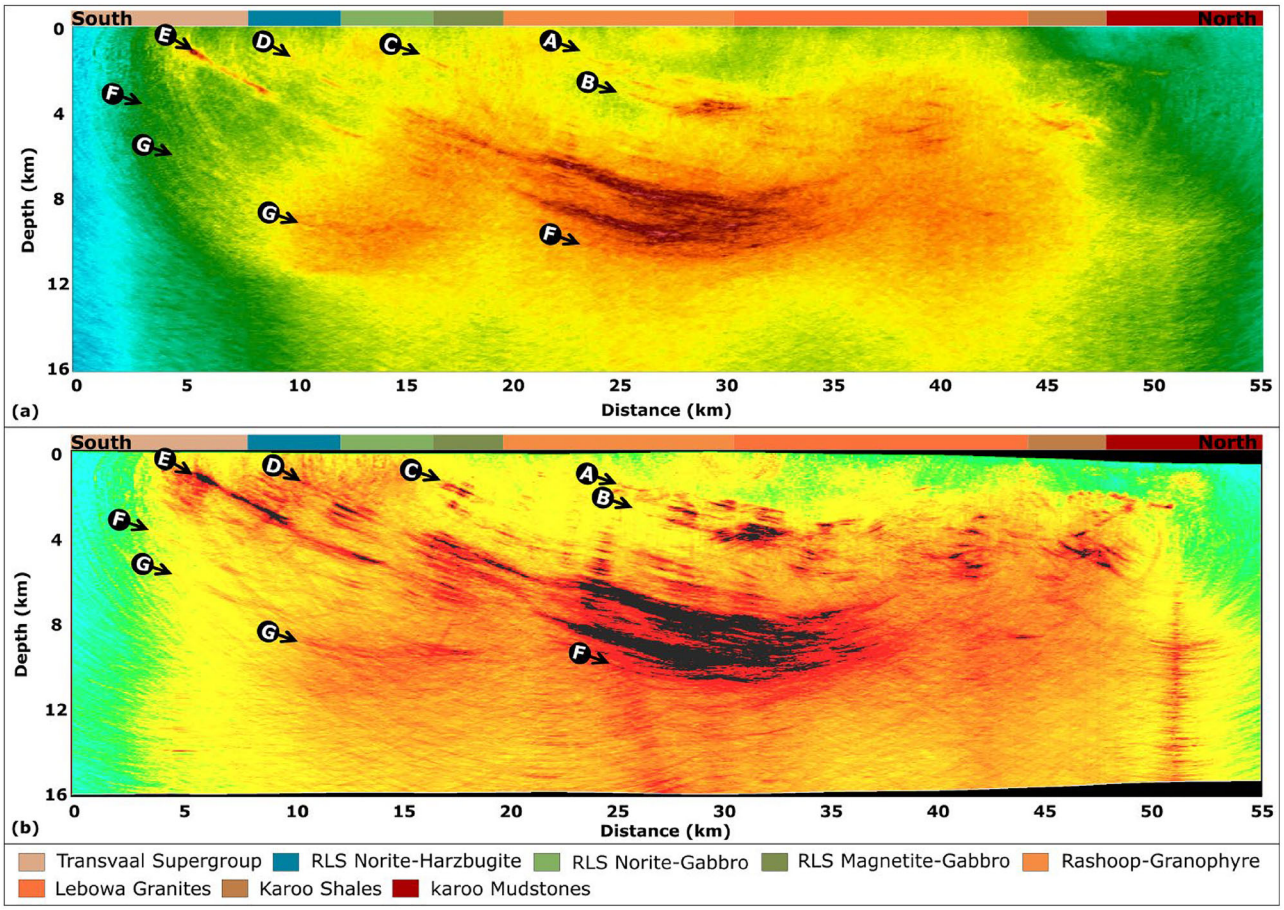


FIGURE 7 (a) Kirchhoff pre-stack depth migration (KPreSDM) section and (b) coherency migration (CM) section, with the main lithological contacts: Rashoop Granophyre-Rustenburg Layered Suite (RLS) ferrogabbros (A), RLS ferrogabbros-RLS gabbros (B), RLS gabbros-RLS norites (C), Transvaal Supergroup-RLS norites (D), a Diabase sill (E), base of Timeball Hill Formation (F), base of Chuniespoort group (G) as well as the geological outcrop along the profile.

it hosts platinum-group element (PGE) deposits in the complex. Our interpretation is constrained by the limitations of 2D seismic data imaging. True dips and thicknesses cannot be determined from 2D data due to signal from out-of-plane reflections that can be misinterpreted as in-plane features. This is exaggerated in hardrock environment with layered igneous rocks of the RLS that might cause seismic energy to scatter, resulting in low amplitude and coherency in the reflections. The interpretation presented in this study is based on constraining data sets (e.g. post-stack time migrated data, regional aeromagnetic data and surface geological mapping) from previous studies. Moreover, the presence of the Karoo sediments on the northern half of the profile leads to high seismic signal energy attenuation. The Karoo Supergroup is laden with dolerite intrusions and has unconsolidated younger sediments, which lead to seismic energy scattering and poor source-to-ground coupling, respectively. Therefore, the interpretation of the data in the northern half is of rather low-confidence, especially without ground truthing constraints (e.g., borehole data).

The anticlinal structure on the seismic section is associated with the Chaneng structure (Figure 10b) in the northern half of the profile. This corresponds to the interpretation of the Chaneng structure by Scheiber-Enslin and Manzi (2018) on the western edge of the Western limb (near Rustenburg). This structure is interpreted to cause shallowing of the PGE mineralization near the intrusive Pilanesberg complex, and it is linked with the updoming of basement rocks during the intrusion of the Bushveld Complex (Scheiber-Enslin & Manzi, 2018). Campbell (2011) interpreted the northern sector of a seismic profile (traversing 50 km NNE from Rustenburg) as a complex graben-like structure where it is crosscut by the Chaneng structure. In this study, the anticlinal structure is interpreted to be a southern extension of the Crocodile River dome covered by younger Karoo sediments.

The target Merensky and UG2 reefs have a thicknesses below 1.5 m and cannot be directly resolved using surface reflection seismic. Therefore, we use the reflections from footwall and hanging wall rocks with significant acoustic impedance contrast to constrain their geometry (Scheiber-

13652478, 2024, 7, Downloaded from https://onlinelibrary.wiley.com/doi/10.1111/1365-2478.13569 by South African Medical Research, Wiley Online Library on [30/11/2024]. See the Terms and Conditions (https://onlinelibrary.wiley.com/terms-and-conditions) on Wiley Online Library for rules of use; OA articles are governed by the applicable Creative Commons License

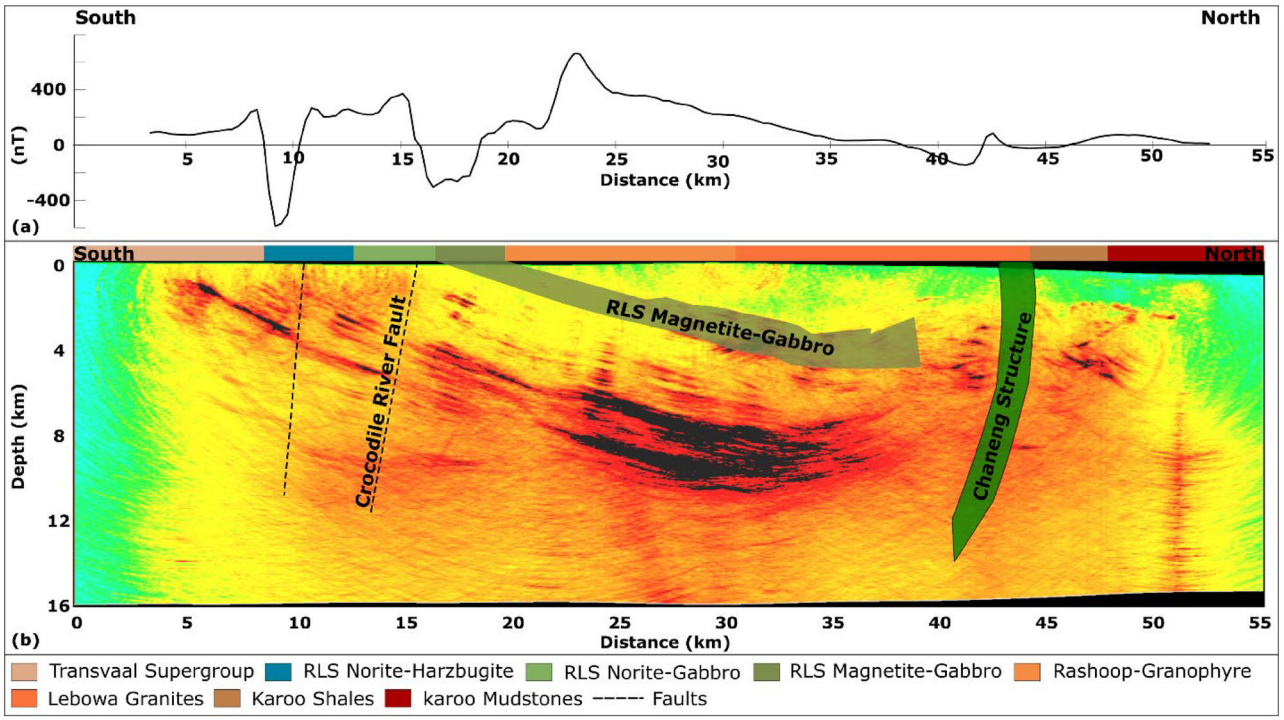


FIGURE 8 (a) Aeromagnetic profile along the (b) coherency migration (CM) section, with the geological features mapped by magnetic data overlain.

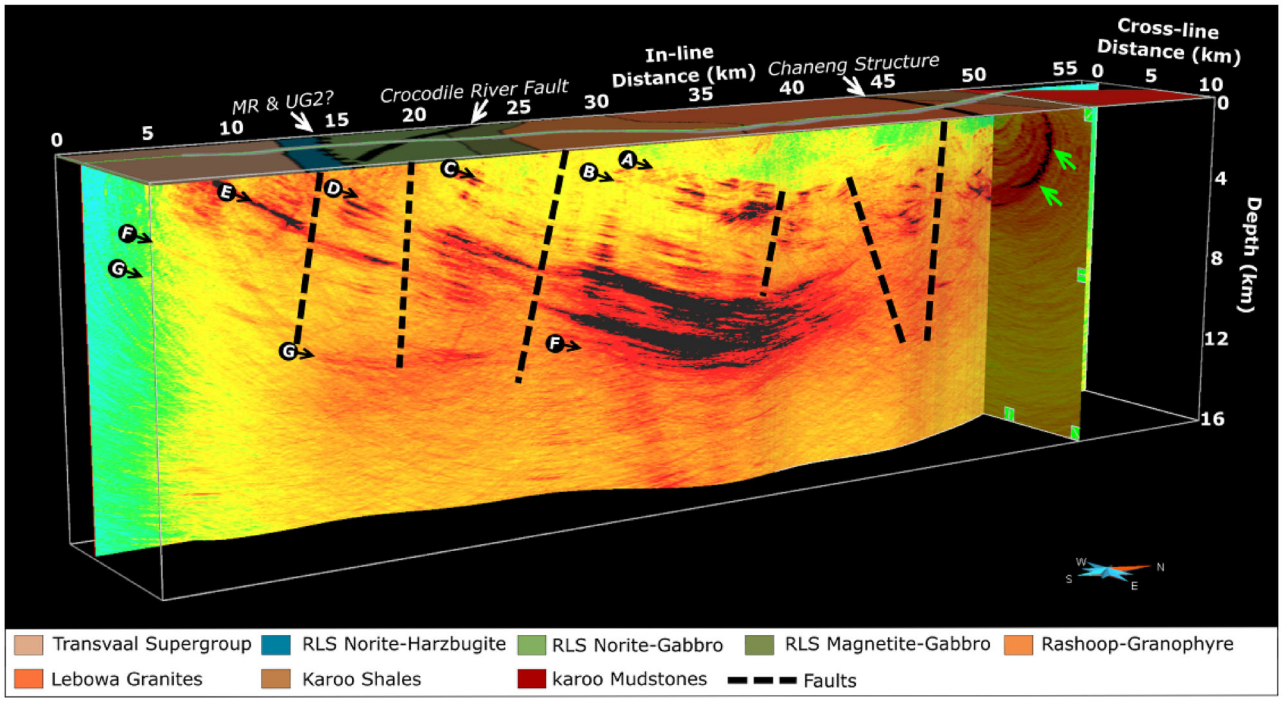


FIGURE 9 3D view of the coherency migration (CM) section with the overlying surface geology showing the regional structures (Chaneng Structure and Crocodile River Fault), and the Merensky reef (MR) and UG2 possible outcrop. The main lithological contacts: Rashoop Granophyre-Rustenburg Layered Suite (RLS) ferrogabbros (A), RLS ferrogabbros-RLS gabbros (B), RLS gabbros-RLS norites (C), Transvaal Supergroup-RLS norites (D), a Diabase sill (E), base of Timeball Hill Formation (F), base of Chuniespoort group (G) as well as the geological outcrop along the profile are shown. The green arrows show constructive interference out-of-plane.

13652478, 2024, 7, Downloaded from https://onlinelibrary.wiley.com/doi/10.1111/1365-2478.13569 by South African Medical Research, Wiley Online Library on [30/11/2024]. See the Terms and Conditions (https://onlinelibrary.wiley.com/terms-and-conditions) on Wiley Online Library for rules of use; OA articles are governed by the applicable Creative Commons License

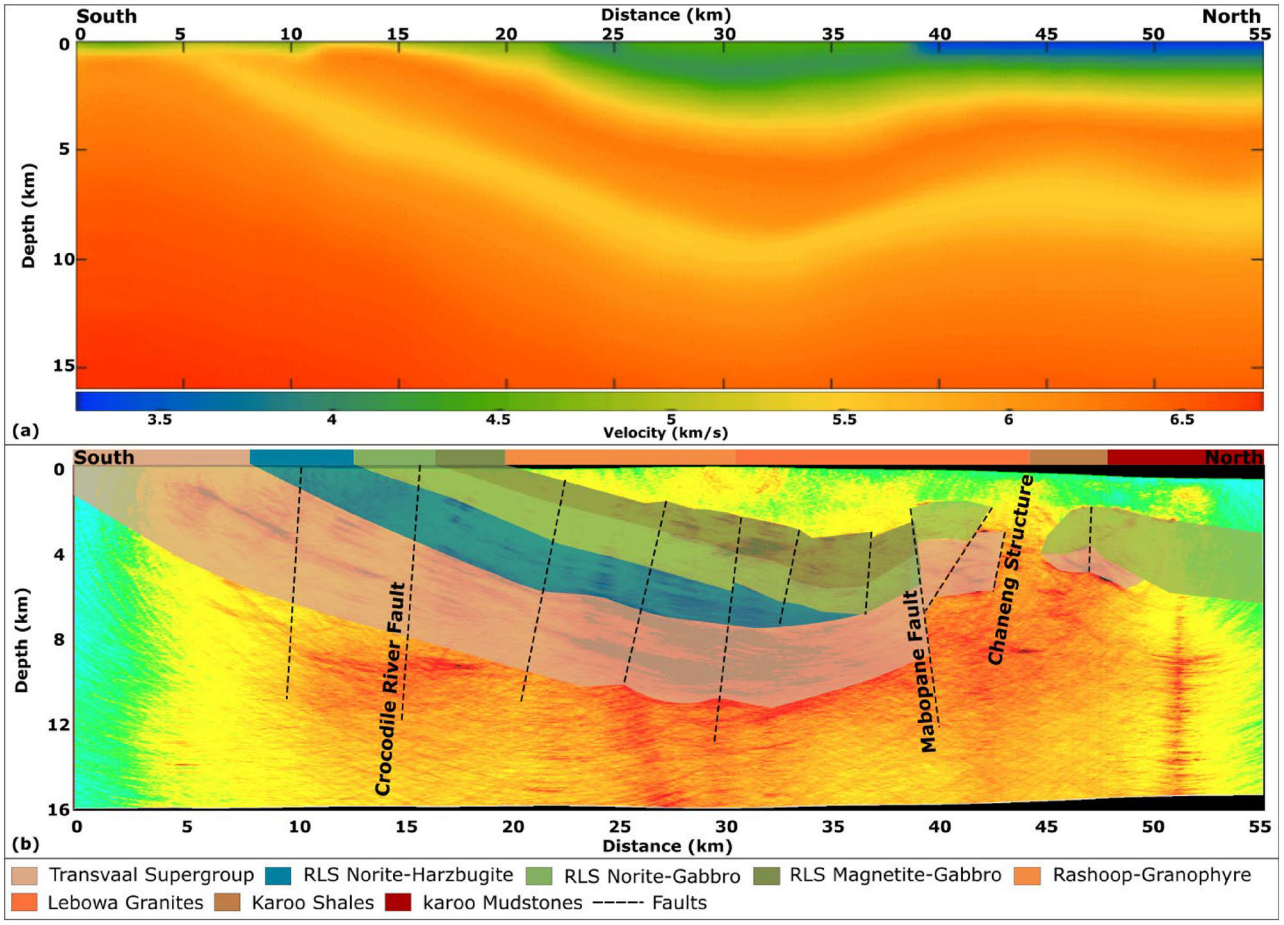


FIGURE 10 The migration velocity model (a) and the final interpreted section (b).

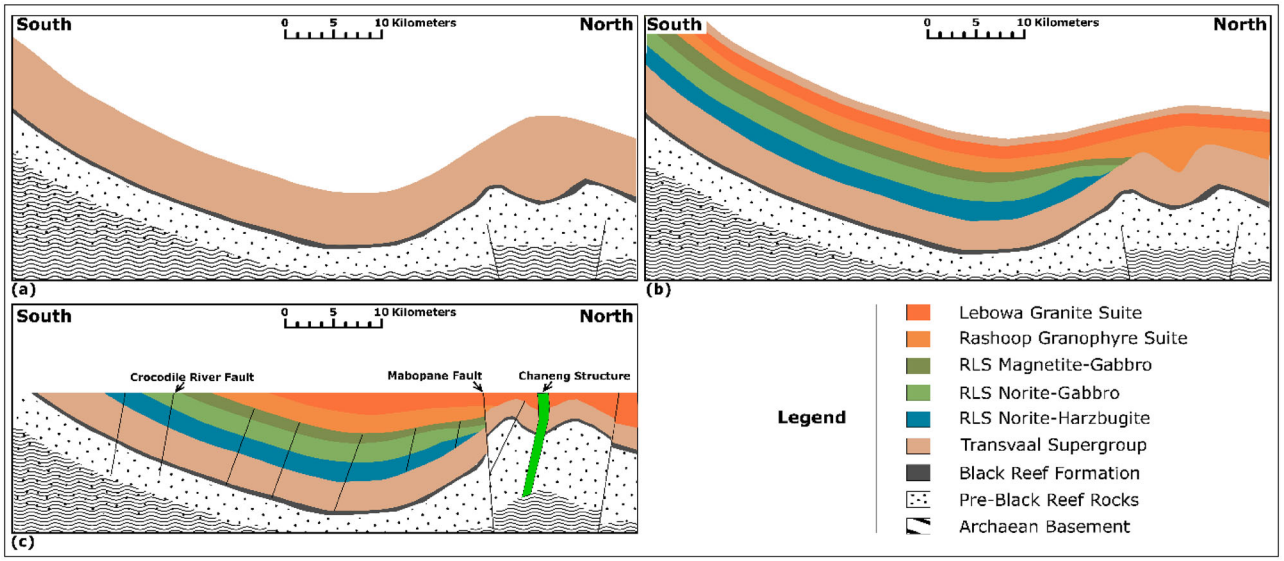


FIGURE 11 Schematic proposed tectonic model along the 2D legacy reflection seismic profile, where (a) shows the Pre-Bushveld Complex deformation, (b) shows the Bushveld Complex intrusion, and (c) shows the Post-Bushveld Complex deformation.

13652478, 2024, 7, Downloaded from https://onlinelibrary.wiley.com/doi/10.1111/1365-2478.13569 by South African Medical Research, Wiley Online Library on [30/11/2024]. See the Terms and Conditions (https://onlinelibrary.wiley.com/terms-and-conditions) on Wiley Online Library for rules of use; OA articles are governed by the applicable Creative Commons License

Enslin & Manzi, 2018). These reefs are interbedded within the RLS norite-harzburgites and the RLS norite-gabbros.

Tectonic model

Our reprocessing results, integrated with existing geological information, were used to constrain the strato-structural model of the region. Transvaal Supergroup sedimentation started approximately 2642 Ma (Walraven & Martini, 1995) with the deposition of the Wachteenbeetje Formation along a series of east-northeasterly trending depressions. Thereafter, thin fluvial sheet sandstones of the Black Reef Formation was deposited, followed by a series of regressions and transgressions events that triggered the development of a shallow shelf in which carbonate and banded iron formations were deposited to produce the Chuniespoort Group rocks (~2557 ± 49–2430 Ma) (Eriksson et el. et al., 2002; Nelson et al., 1999). Following a period of erosion and marine transgression, Pretoria Group siliciclastic sedimentary rocks were deposited, approximately 2224 ± 21 Ma (Eriksson et al., 2002; Hartzer, 1989; Walraven & Martini, 1995).

Pre-Bushveld Complex deformation that followed the Transvaal Supergroup deposition includes, first, updoming of the sediments that resulted in the deposition of thinner Pretoria Group sediments in the Crocodile River dome area. Second, the development of northwest striking folds, followed by east-northeast striking folds from compressional forces. Finally, possible faulting along weak zones, as shown by the south-north tectonic model along the legacy profile (Figure 11a) (Hartzer, 1989).

The Bushveld Complex intrusion into the upper Pretoria Group rocks at approximately 2055 Ma terminated the sedimentation of the Transvaal Supergroup. The location of the feeders and the exact composition of the parental magmas are still subject to debate. The coarse-grained Bushveld igneous rocks with composition ranging from ultramafic to felsic were emplaced from different feeder channels and their rate and effective mixing are yet to be resolved. The updoming of the Transvaal rocks advanced to a stage where the domes acted as barriers, controlling the magma to either spread out against them or extend across, as shown in Figure 11b. The intrusion reactivated pre-existing deformation structures and caused low-medium grade metamorphism in the Transvaal sediments (Hartzer, 1989).

Post-Bushveld Complex deformation reactivated the northwest and east-northeast striking seismically-defined fault zones such as the Crocodile River fault and Chaneng structure, respectively. Isostatic readjustment due to the intrusion probably exerted further compressional forces on the folds, leading to a relative upward movement of the Transvaal inlier (Crocodile River dome) and subsequent erosion (Figure 11c) (Hartzer, 1989).

CONCLUSION

Reprocessing of the 2D legacy seismic profile using coherency migration (CM) has yielded an improved depth image of the geological structures of the Western limb of the Bushveld Complex. Despite the challenges associated with seismic energy attenuation, the platinum group element (PGE) bearing horizons of the Rustenburg Layered Suite (RLS) have been imaged with considerable confidence. Moreover, the information from the previous seismic, magnetic and geological studies in the Bushveld complex has contributed to the imaging of the complex geological structures. The aeromagnetic data were used for the first time to constrain the interpretation of the profile. Previous studies had no conclusive results on the northern half of the profile due to low resolution imaging in this section. The low signal-to-noise ratio (SNR) in the northern half of the profile is attributed to the presence of out-of-plane reflectivity. Despite the presence of out-of-plane reflectivity, the SNR of the northern half of the profile has been improved.

The northern half of the profile interpretation provides evidence for the presence of the geological structures interpreted in the previous studies, namely Mabopane fault and Chaneng structure. The anticlinal structure present in the northern half of the profile was successfully imaged by the CM technique. The updoming and erosion of the RLS lithologies provide possible evidence of reduction of PGE mineralization in this region. The tectonic evolution outlined along the profile provides insight into the possible depletion of the PGE mineralization in the northern edge of the profile. A 3D reflection seismic acquisition method is recommended to improve the SNR of the northern edge of the profile to account for out-of-plane reflectivity.

ACKNOWLEDGEMENTS

We are grateful for the financial support from DST-NRF CIMERA and Wits Seismic Research Centre. The coordinates were sorted on MATLAB and pre-stack time domain seismic data reprocessing was done on the Globe Claritas; we appreciate the sponsorship of the software licences by Globe Claritas to the University of the Witwatersrand, Johannesburg. We acknowledge the Council of Geoscience for providing access to the raw seismic data for the study.

DATA AVAILABILITY STATEMENT

The data that support the findings of this study are available from the corresponding author upon reasonable request.

ORCID

Mpofana Sihoyiya https://orcid.org/0000-0003-1956-5223
Musa S. D. Manzi https://orcid.org/0000-0002-1654-5211
Moyagabo K. Rapetsoa https://orcid.org/0000-0003-3275-8994

13652478, 2024, 7, Downloaded from https://onlinelibrary.wiley.com/doi/10.1111/1365-2478.13569 by South African Medical Research, Wiley Online Library on [30/11/2024]. See the Terms and Conditions (https://onlinelibrary.wiley.com/terms-and-conditions) on Wiley Online Library for rules of use; OA articles are governed by the applicable Creative Commons License

REFERENCES

Akingboye, A.S. & Ogunyele, A.C. (2019) Insight into seismic refraction and electrical resistivity tomography techniques in subsurface investigations. *Rudarsko-geološko-naftni zbornik (The Mining-Geological-Petroleum Engineering Bulletin)*, 34(1), 93–111. https://doi.org/10.17794/rgn.2019.1.9

Basson, I.J. (2019) Cumulative deformation and original geometry of the Bushveld Complex. *Tectonophysics*, 750, 177–202. https://doi.org/10.1016/j.tecto.2018.11.004

Bleistein, N. (1984) *Mathematical methods for wave phenomena*. New York: Academic Press Inc.

Buske, S. (1999) Three-dimensional pre-stack Kirchhoff migration of deep seismic reflection data. *Geophysical Journal International*, 137, 243–260. https://doi.org/10.1046/j.1365-246x.1999.00789.x

Buske, S., Gutjahr, S. & Sick, C. (2009) Fresnel volume migration of single-component seismic data. *Geophysics*, 74(6), WCA47–WCA55. https://doi.org/10.1190/1.3223187

Bräunig, L., Buske, S., Malehmir, A., Bäckström, E., Schön, M. & Marsden, P. (2019) Seismic depth imaging of iron-oxide deposits and their host rocks in the Ludvika mining area of central Sweden. *Geophysical Prospecting*, 68(1), 24–43. https://doi.org/10.1111/1365-2478.12836

Campbell, G. (2011) Exploration geophysics of the Bushveld Complex in South Africa. *The Leading Edge*, 30(6), 622–638. https://doi.org/10.1190/1.3599148

Cawthorn, R.G. (1999) The discovery of the platiniferous Merensky Reef in 1924. *South African Journal of Geology*, 102(3), 178–183. https://hdl.handle.net/10520/EJC-112518d32d

Cawthorn, R.G. & Webb, S.J. (2001) Connectivity between the western and eastern limbs of the Bushveld Complex. *Tectonophysics*, 330(3–4), 195–209. https://doi.org/10.1016/S0040-1951(00)00227-4

Cheraghi, S., Hloušek, F., Buske, S., Malehmir, A., Adetunji, A., Haugaard, R., Snyder, D. & Vayavur, R. (2022) Reflection seismic imaging across a greenstone belt, Abitibi (Ontario)-Canada. *Geophysical Prospecting*, 71, 1096–1115. https://doi.org/10.1111/1365-2478.13284

Donoso, G.A., Malehmir, A., Pacheco, N., Araujo, V., Penney, M., Carvalho, J., Spicer, B. & Beach, S. (2020) Potential of legacy 2D seismic data for deep targeting and structural; imaging at the Neves-Corvo massive sulphide-bearing deposit, Portugal. *Geophysical Prospecting*, 68, 44–61. https://doi.org/10.1111/1365-2478.12861

Du Plessis, A. & Levitt, J.G. (1987) *On the structure of the Rustenburg Layered Suite—Insight from seismic reflection data. Presented at the Indaba on the tectonic setting of layered intrusives*. Johannesburg: Geological Society of South Africa.

Durrheim, R.J. (2015) Structural seismology: investigations of the crust and mantle. In: de Beer, J.H. (Eds.), *The history of geophysics in Southern Africa*. Johannesburg: South African Geophysical Association, pp. 165–189.

Eriksson, P.G., Condie, K.C., Westhuizen, W.V.D., Merwe, R.V.D., Bruiyn, H.D., Nelson, D.R., Altermann, W., Catuneanu, O., Bumby, A.J., Lindsay, J. & Cunningham, M.J. (2002) Late Archaean superplume events: a Kaapvaal-Pilbara perspective. *Journal of Geodynamics*, 34, 207–247. https://doi.org/10.1016/S0264-3707(02)00022-4

Hartzer, F.J. (1989) Stratigraphy, structure and tectonic evolution of the Crocodile River Fragment. *South African Journal of Geology*, 92, 110–124.

Hartzer, F.J. (1995) Transvaal Supergroup inliers: geology, tectonic development and relationship with the Bushveld Complex, South Africa. *Journal of African Earth Sciences*, 21(4), 521–547. https://doi.org/10.1016/0899-5362(95)00108-5

Heinonen, S., Malinowski, M., Hloušek, F., Gislason, G., Buske, S., Koivisto, E. & Wojdyla, M. (2019) Cost-effective seismic exploration: 2D reflection imaging at the Kylylahti massive sulfide deposit, Finland. *Minerals*, 9(5), 263. https://doi.org/10.3390/min9050263

Hloušek, F., Malinowski, M., Bräunig, L., Buske, S., Malehmir, A., Markovic, M., Sito, L., Marsden, P. & Bäckström, E. (2022) Three-dimensional reflection seismic imaging of the iron oxide deposits in the Ludvika mining area, Sweden, using Fresnel volume migration. *Journal of Geophysical Research: Solid Earth*, 13(5), 917–934. https://doi.org/10.5194/se-13-917-2022

Hloušek, F., & Buske, S. (2016). Fresnel volume migration of the ISO89-3D data set. *Geophysical Supplements to the Monthly Notices of the Royal Astronomical Society*, 207(2), 1273–1285. https://doi.org/10.1093/gji/ggw336

Hloušek, F., Hellwig, O. & Buske, S. (2015a) Improved structural characterization of the Earth's crust at the German Continental Deep Drilling Site using advanced seismic imaging techniques. *Journal of Geophysical Research: Solid Earth*, 120(10), 6943–6959. https://doi.org/10.1002/2015JB012330

Hloušek, F., Hellwig, O. & Buske, S. (2015b) Three-dimensional focused seismic imaging for geothermal exploration in crystalline rock (Schneeberg, Germany). *Geophysical Prospecting*, 63(4), 999–1014. https://doi.org/10.1111/1365-2478.12239

Hua, B. & McMechan, G. (2009) Parsimonious Kirchhoff depth migration. *Journal of Seismic Exploration*, 18, 157–179.

Humphrey, W.A. (1906) On a portion of the Bushveld lying south of the Rooiberg and east of the Crocodile river. In: *Geological Survey, Transvaal, Pretoria, South Africa*. Annual Report*, 1906*. Geological Survey Transvaal, pp. 109–115.

Humphrey, W.A. (1909) On a portion of the Bushveld bordering the Crocodile River and including the Rooiberg tin-field. *Geological Survey Transvaal, Pretoria, South Africa*. Reporter*, 1908*. Geological Survey Transvaal, pp. 103–112.

Jusri, T., Bertani, R. & Buske, S. (2018) Advanced three-dimensional seismic imaging of deep supercritical geothermal rocks in Southern Tuscany. *Geophysical Prospecting*, 67(2), 298–316. https://doi.org/10.1111/1365-2478.12723

Lüth, S., Buske, S., Giese, R. & Goertz, A. (2005) Fresnel volume migration of multicomponent data. *Geophysics*, 70(6), S121–S129. https://doi.org/10.1190/1.2127114

Malehmir, A., Donoso, G., Markovic, M., Maries, G., Dynesius, L., Brodic, B., Pecheco, N., Marsden, P., Bäckström, E., Penney, M. & Araujo, V. (2019) Smart exploration: from legacy data to state-of-the-art data acquisition and imaging. *First Break*, 37(8), 71–74. https://doi.org/10.3997/1365-2397.n0049

Malehmir, A. & Bellefleur, G. (2010) Reflection seismic imaging and physical properties of base-metal and associated iron deposits in the Bathurst Mining Camp, New Brunswick, Canada. *Ore Geology Reviews*, 38(4), 319–333. https://doi.org/10.1016/j.oregeorev.2010.08.002

Manzi, M.S.D., Cooper, G.R.J., Malehmir, A. & Durrheim, R.J. (2019) Improved structural interpretation of legacy 3D seismic data from Karee platinum mine (South Africa) through the application of novel

13652478, 2024, 7, Downloaded from https://onlinelibrary.wiley.com/doi/10.1111/1365-2478.13569 by South African Medical Research, Wiley Online Library on [30/11/2024]. See the Terms and Conditions (https://onlinelibrary.wiley.com/terms-and-conditions) on Wiley Online Library for rules of use; OA articles are governed by the applicable Creative Commons License

seismic attributes. *Geophysical Prospecting*, 68(1), 145–163. https://doi.org/10.1111/1365-2478.12900

Manzi, M., Malehmir, A. & Durrheim, R. (2019) Giving the seismic data the attention they deserve. *First Break*, 37(8), 89–96. https://doi.org/10.3997/1365-2397.n0050

Nedimović, M.R. & West, G.F. (2003) Crooked-line 2D seismic reflection imaging in crystalline terrains: part 2, migration. *Geophysics*, 68(1), 286–296. https://doi.org/10.1190/1.1543214

Neidell, N.S. & Taner, M.T. (1971) Semblance and other coherency measured for multichannel data. *Geophysics*, 36(3), 482–497. https://doi.org/10.1190/1.1440186

Nelson, D.R., Trendall, A.F. & Altermann, W. (1999) Chronological correlations between the Pilbara and Kaapvaal cratons. *Precambrian Research*, 97, 165–189. https://doi.org/10.1016/S0301-9268(99)00031-5

Odgers, A.T.R., Hinds, R.C. & Von Gruenewaldt, G. (1993) Interpretation of a seismic reflection survey across the southern Bushveld Complex. *South African Journal of Geology*, 96, 205–212.

Potgieter, G.S. & Malan, D.F. (2010) Preliminary evaluation of the proposed mining method at Eland Platinum Mine. In: *The 4th International Platinum Conference*, Platinum in transition 'Boom or Bust'. Johannesburg, The Southern African Institute of Mining and Metallurgy, pp. 345–352.

Pretorius, C.C., Muller, M.R., Larroque, M. & Wilkins, C. (2003) A review of 16 years of hardrock seismic of the Kaapvaal Craton. In: Eaton D.W., Milkereit B., & Salisbury M.H. (Eds.) *Hardrock seismic exploration, geophysical developments*. Houston, Society of Exploration Geophysicists, pp. 247–268. https://doi.org/10.1190/1.9781560802396.ch16

Pretorius, C.C., Trewick, W.F., Fourie, A. & Irons, C. (2000) Application of 3D-seismics to mine planning at the Vaal Reefs gold mine, number 10 shaft, republic of South Africa. *Geophysics*, 65, 1862–1870. https://doi.org/10.1190/1.1444870

Rapetsoa, M.K., Manzi, M.S.D., Westgate, M., Sihoyiya, M., James, I., Onyebueke, E., Kubeka, P., Durrheim, R.J. & Kgarume, T. (2022) Cost-effective in-mine seismic experiments to image platinum deposits and associated geological structures at Maseve platinum mine, South Africa. *Near Surface Geophysics*, 20(6), 572–589. https://doi.org/10.1002/nsg.12216

Riedel, M., Dutsch, C., Alexandrakis, C., Dini, I., Ciuffi, S. & Buske, S. (2015) Seismic depth imaging of a geothermal system in southern Tuscany. *Geophysical Prospecting*, 63(4), 957–974. https://doi.org/10.1111/1365-2478.12254

Scheiber-Enslin, S. & Manzi, M. (2018) Integration of 3D reflection seismics and magnetic data for deep platinum mine planning and risk mitigation: a case study from Bushveld Complex, South Africa. *Exploration Geophysics*, 49(6), 928–939. https://doi.org/10.1111/1365-2478.12254

Schreiter, L., Hloušek, F., Hellwig, O. & Buske, S. (2015) Characterization of seismic reflections from faults in a crystalline environment, Schneeberg, Germany. *Geophysical Prospecting*, 63(4), 1015–1032. https://doi.org/10.1111/1365-2478.12255

Schneider, W.A. (1978) Integral formulation for migration in two and three dimensions. *Geophysics*, 43, 49–76. https://doi.org/10.1190/1.1440828

Sehoole, L., Manzi, M.S.D., Zhang, S.E. & Bourdeau, J.E. (2020) An innovative seismic and statistical approach to understand 3D magmatic structures and ore deposits in the western Bushveld Complex, South Africa. *Ore Geology Reviews*, 126, 103784. https://doi.org/10.1016/j.oregeorev.2020.103784

Shithigona, O., Manzi, M.S.D., Ashwal, L.D., Bybee, G.M. & Webb, S.J. (2018) Experimental studies of elastic wave velocities and densities in rocks from the Bushveld Complex, South Africa: implications for deep reflection seismic surveys. *South African Journal of Geology*, 121(3), 311–326. https://doi.org/10.25131/sajg.121.0029

Sihoyiya, M., Manzi, M.S.D., James, I., Rapetsoa, M.K., Westgate, M., Nwaila, G., Linzer, L., Durrheim, R.J. & Staley, P. (2022) Seismic delineation of the gold-bearing structures in the South Rand Goldfield (South Africa)—Comparison of pre-stack time and depth migration approaches on legacy seismic data. *Near Surface Geophysics*, 20(6), 697–709. https://doi.org/10.1002/nsg.12209

Singh, B., Malinowski, M., Hloušek, F., Koivisto, E., Heinonen, S., Hellwig, O., Buske, S., Chamarczuk, M. & Juurela, S. (2019) Sparse 3D seismic imaging in the Kylylahti mine area, Eastern Finland: comparison of time versus depth approach. *Minerals*, 9(5), 305. https://doi.org/10.3390/min9050305

Sun, H. & Schuster, G.T. (2003) 3D wavepath migration. *Geophysical Prospecting*, 51, 421–430. https://doi.org/10.1046/j.1365-2478.2003.00380.x

Tabti, H., Gelius, L.J. & Hellmann, T. (2004) Fresnel-aperture prestack depth migration. *First Break*, 22, 39–48. https://doi.org/10.3997/1365-2397.2004005

Takahashi, T. (1995) Prestack migration using arrival angle information. *Geophysics*, 60, 154–163. https://doi.org/10.1190/1.1443742

Tillmanns, M., Simon, M., Zitzelsberger, A. & Gebrande, H. (1996) Neue Seismographien aus dem Umfeld der Kontinentalen Tiefbohrung (KTB), Oberpfalz, *Geol. Bavarica*, 101, 291–314.

Tillmanns, M. & Gebrande, H. (1999) Focusing in prestack isochron migration using instantaneous slowness information. *Pure and Applied Geophysics*, 156, 187–206.

Walraven, F. & Martini, J. (1995) Zircon Pb-evaporation age determinations of the Oak Tree Formation, Chuniespoort Group, Transvaal Sequence: implications for Transvaal-Griqualand West basin correlations. *South African Journal of Geology*, 96, 58–67. https://hdl.handle.net/10520/EJC-929187cc0

Westgate, M., Manzi, M.S.D., James, I. & Harrison, W. (2020) New insight from legacy seismic data: reprocessing of legacy 2D seismic data for imaging of iron-oxide mineralization near Sishen Mine, South Africa. *Geophysical Prospecting*, 68(7), 2119–2140. https://doi.org/10.1111/1365-2478.12996

Woodward, D.J. (1991) *Inversion of seismic refraction data*. Geophysics Division Technical Report No. 114.

Zhang, J. & Toksöz, M.N. (1998) Nonlinear refraction traveltime tomography. *Geophysics*, 63(5), 1726–1737. https://doi.org/10.1190/1.1444468

How to cite this article: Sihoyiya, M., Hloušek, F., Manzi, M.S.D., Rapetsoa, M.K., Buske, S. & Khoza, D. (2024) Seismic imaging of the complex geological structures in the southwestern edge of the Western limb, Bushveld Complex through focusing pre-stack depth migration of legacy 2D seismic data. *Geophysical Prospecting*, 72, 2504–2519. https://doi.org/10.1111/1365-2478.13569

13652478, 2024, 7, Downloaded from https://onlinelibrary.wiley.com/doi/10.1111/1365-2478.13569 by South African Medical Research, Wiley Online Library on [30/11/2024]. See the Terms and Conditions (https://onlinelibrary.wiley.com/terms-and-conditions) on Wiley Online Library for rules of use; OA articles are governed by the applicable Creative Commons License